Broadband mesoscopic optoacoustic tomography reveals skin layers

J. Aguirre,* M. Schwarz, D. Soliman, A. Buehler, M. Omar, and V. Ntziachristos

Institute for Biological and Medical Imaging, Technische Universität München and Helmholtz Zentrum München, Neuherberg D85764, Germany

**Corresponding author: juanaguir@gmail.com*

Received July 22, 2014; revised September 29, 2014; accepted September 30, 2014; posted October 7, 2014 (Doc. ID 217546); published 0 MONTH 0000

We have imaged for the first time to our knowledge human skin *in vivo* with a raster-scan optoacoustic mesoscopy system based on a spherically focused transducer with a central frequency of 102.8 MHz and large bandwidth (relative bandwidth 105%). Using tissue phantoms we have studied the ability of the system to image vessels of sizes within the anatomically significant range from the key anatomical vasculature sites. The reconstructed images from experiments *in vivo* show several structures from the capillary loops at the dermal papillae, the horizontal plexus, and the difference between the dermis and the epidermis layers.

OCIS codes: (110.0110) Imaging systems; (170.5120) Photoacoustic imaging; (170.1610) Clinical applications.

http://dx.doi.org/10.1364/OL.99.099999

Histopathological analysis of biopsied skin is an invasive, slow, and expensive medical process in dermatology, but necessary for accurately diagnosing skin diseases [1]. State-of-the-art skin optical-imaging techniques like dermoscopy or linear and nonlinear microscopy methods are proposed as an alternative to reduce the number of biopsies [2–6], but they are intrinsically limited by light scattering, which limits the imaging depth to a few hundred microns. Optical coherence tomography (OCT) may penetrate deeper than dermoscopy or confocal imaging to depths of ~1 mm. However, the skin depth ranges from 1.5 to 4 mm depending on the anatomical site [7] and imaging at such depths is necessary in different pathologies.

Optoacoustic mesoscopy, based on high-frequency acoustic resolution, may be an interesting alternative for skin imaging. Optoacoustic mesoscopy refers to optoacoustic imaging that goes beyond the depth of optical microscopy, reaching several millimeters deep in tissue [8]. Compared to confocal imaging or OCT it also offers alternative contrast mechanisms by resolving the absorption of light by tissue [9,10].

Cross-sectional optoacoustic imaging of the skin has been already demonstrated using a linear array of transducers operating at 24 MHz [11]. The depth of skin lesions and burns was resolved with 97 μm lateral resolution and 22 μm axial resolution. Skin vasculature [12,13] has also been resolved using interferometry [14] or piezoelectric-focused detectors [15,16] operating at central frequencies of up to 50 MHz. The highest lateral resolution achieved so far was ~40 μm, whereas the axial resolution reached ~15 μm. At this resolution, only the larger skin vessels (25–100 μm) are visible, i.e., vessels situated relatively deep in the dermis [17]. Smaller vessels (7–25 μm) situated close to the epidermal-dermal junction [18] blur the images and typically have to be removed for rendering purposes [19]. Most mesoscopy implementations show vascular images as maximum intensity projections along the axial direction (coronal views) of the entire skin, a view that is not favorable to assess lesion depth. Skin imaging with a high-frequency unfocused $LiNbOb_3$ detector has been also considered for skin imaging, yielding lateral resolution of 200 μm [20].

An ultrawideband (20–200 MHz) system, implemented in transillumination, recently achieved ~30 μm lateral and 7 μm an axial resolution [21]. In this work we applied an epi-illumination version of this technology [22] to skin visualization and interrogated whether operation at a broader bandwidth could differentiate skin layers in axial and coronal skin views. In particular, we investigated if features not visible in the 25–50 MHz are better resolved when collecting broader frequency content. Imaging was based on a custom-made 102.8 MHz central frequency spherically focused transducer constructed out of $LiNbOb_3$ to yield ultrawideband measurements ranging from a few millihertz to ~200 MHz. The active element of the transducer had a diameter of 1.5 mm and an f-number of ~1 (numerical aperture ~0.5). The frequency response of the transducer is shown in Fig. 1 Detected optoacoustic signals were preamplified by a low-noise amplifier (63 dB, AU-1291, Mited Inc., Haupppauge, New York, USA) and collected by a high-speed digitizer (CS122G1, Gage, Lockport, Illinois, USA,; 12-bit resolution; max sampling rate, 2GS/S). The detector was raster

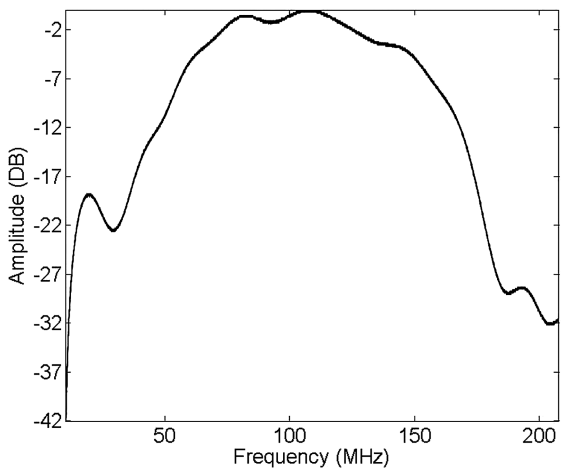

Fig. 1. Frequency spectrum of the transducer. F1:1

scanned in proximity to the skin, as shown in Figs. 2(a) and 3, with its focal point placed ~100 μm above the surface of the imaged region. Three-dimensional image reconstruction was then based on a back-projection algorithm [21]. Skin epi-illumination was achieved using three fiber bundles arranged around the transducer to generate an illumination pattern of ~1 mm in diameter, confocal with the focal point of the transducer [22]. To perform the raster scan fast motorized piezostages were used (M683.2U4, Physik Instrumente GmbH & Co. KG, Karlsruhe, Germany). The illumination light was generated by a 532 nm laser, with a pulse repetition rate of 1 kHz. The energy per pulse was below 1 mJ over ~1 cm^2, fulfilling the safety standards for human use. The temporal width of the pulse was of 0.9 ns. The pulse duration is critical for imaging small structures, since the stress confinement condition must be fulfilled [20]. We have previously shown that the illumination parameters employed herein can lead to axial resolutions of 4 μm [21].

The system performance was first examined with two phantoms. Phantom 1 assessed the frequency profile detected from small structures resembling small skin capillaries placed near the epidermal-dermal junction. Phantom 1, shown in Fig. 2(a), consisted of a surgical suture 10 μm in diameter, placed at different depths within pork tissue. Figure 2(b) shows the frequency response detected from the suture placed at different depths. The figure shows that there is significant signal contained at frequencies that are larger than 100 MHz, which indirectly indicates that systems in the 25–50 MHz range may miss such fine information. As expected, the high-frequency signal reduces as the suture is moved deeper, due to the frequency-dependent attenuation of sound waves in tissue. For depths of 300 μm, corresponding to the location of the epidermal-dermal junction in thick skin, frequencies above 100 MHz are still measured. Interestingly, even for depths of 800 μm, significant contributions above 50 MHz can be measured.

Phantom 2 was built to assess the ability of the transducer to capture lower-frequency signals corresponding to larger skin vessels. It consisted of a surgical suture 100 μm in diameter under the tissue surface. The exact placement depth of the suture in this case would impose less of an issue, due to reduced acoustic attenuation of the lower ultrasound frequencies generated; therefore a single depth at 120 μm was studied. Figure 2(c) depicts the frequency response of the 100-μm-diameter suture. As expected, significantly lower frequency content is exhibited in this case. The ultrabandwidth collection ability of the transducer recorded signals of few millihertz to tens of millihertz. This finding illustrates that the technology employed herein is appropriate for detecting a large variation of feature sets in the skin.

To elucidate the performance of ultrawideband optoacoustic mesoscopy on skin, we imaged a 5 mm × 5 mm region in the palm of a healthy male volunteer. A specific interface was built to acoustically couple the transducer to the skin. It consisted of a cubic glass enclosure with a 2 cm × 2 cm opening in its bottom, which was sealed with an optically and acoustically transparent film. The enclosure was placed in direct contact with the skin for data acquisition. The enclosure was filled with water to enable sound coupling to the detector, as shown in Fig. 3. The step size of the raster scan was 10 μm along the x and y direction (Fig. 4). The voxel size in the reconstructed 3D volume was set to 10 μm × 10 μm × 2.5 μm. Prior to reconstruction, the acquired data was filtered using a 1–200 MHz bandpass filter. Figure 4 depicts an axial slice of the reconstructed image. The epidermis layer can be clearly distinguished; its width is ~200 μm, which is in accordance with previously published values for the thickness of the epidermis in the palm hand [13]. Below the epidermis junction begins the area in which the capillary loops are situated. Although the numerical aperture of the detector is high, vessels whose direction is not perpendicular enough to the axial axis of the transducer do not appear in the reconstructed image, due to the strong directivity of the optoacoustic signals [23]. Therefore, only a part of the capillary loops appear in the reconstructions. The vessels situated deeper in the horizontal plexus appear clearly in the reconstruction.

Figure 5 shows three maximum-intensity projections (MIP) parallel to the skin surface, taken at different depths. The top MIP corresponds to the epidermal-dermal junction. The bright dots are in agreement with the top part of the capillaries. The stripes correspond

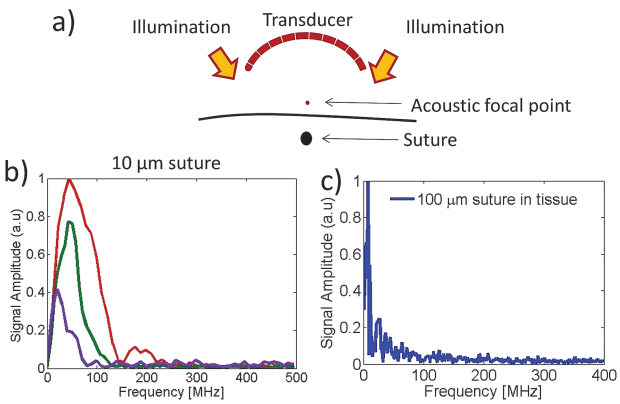

Fig. 2. (a) Scheme of the acquisition setup for phantom 1 and 2. (b) Frequency content of the signal measured from a 10 μm suture inserted at 3 different depths in tissue (phantom 1) measured with the 102.8 MHz transducer. (c) Frequency content of the incoming signal from a 100 μm suture measured with the 102.8 MHz transducer.

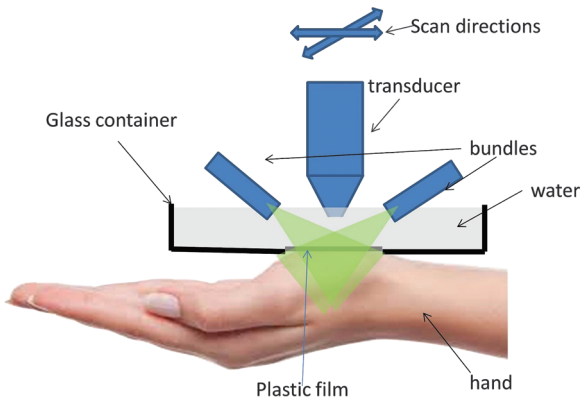

Fig. 3. Schematic of the acquisition setup for the hand experiment. The focal point of the transducer is placed slightly above the surface of the skin. The glass container filled with water allows to acoustically couple the skin with the transducer.

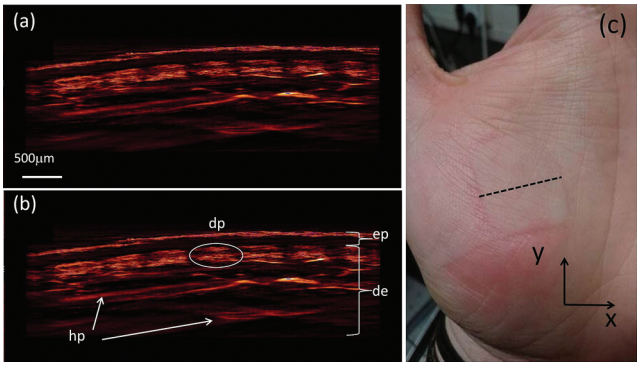

Fig. 4. (a)(b) Axial slice taken from the reconstruction of the data acquired from the hand palm with and without indications. (c) Photo of the palm hand from which the *in vivo* data was acquired. The square in which the raster scan was performed can be seen. The dotted line corresponds to the slice shown in Right Abbreviations: ep—epidermis; de—dermis; dp—dermal papillae; hp—horizontal plexus.

to the shape of dermal papillae, which in the palm of the hand follows the same shape of the outer epidermal ridges [24]. The image of the middle MIP is in agreement with the smaller vessels of the horizontal plexus situated closer to the epidermal-dermal junction and the connections between capillary loops. The bigger vessels located below in the horizontal plexus appear clearly in the lower MIP.

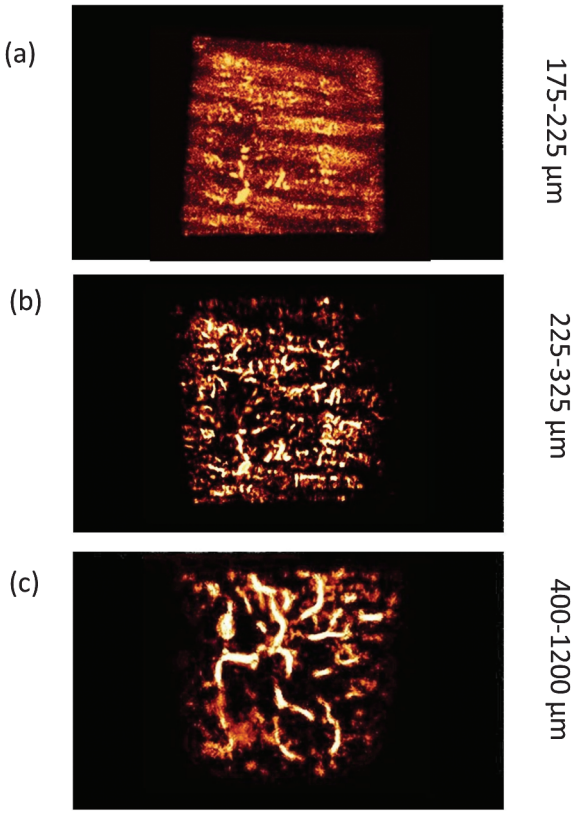

Fig. 5. (a),(b),(c) MIPS of the reconstructed image in the direction perpendicular to the skin surface. The values on the right represent the approximate minimum depth and maximum depth used for the calculation of each projection.

Most of the skin vasculature is organized in a horizontal plexus, situated at 1–2 mm below the skin, at the papillary dermis zone. From the horizontal plexus arterial capillaries ascend up to the epidermal-dermal junction to form the dermal capillary loops that provide nutrients to the dermal papillae [17]. The diameters of the vessels that form the capillary loops range from 7 to 11 µm. The system employed herein could clearly visualize the epidermal-dermal junction, situated at depths around 80 µm for thin skin and 300 µm for thick skin [18]. In the horizontal plexus, most of the vessel diameters are in the range of 17–26 µm. In the mid- and deep-dermis vessels are larger, up to a maximum of 100 µm in diameter [17]. The 100 MHz raster-scan system employed herein was shown capable of highly scalable skin imaging. Scalability herein implies that the system could detect the incoming high-frequency signal from the ~10 µm vessels situated close to the epidermal-dermal junction and the lower-frequency ultrasound signals generated by the larger vessels situated in the lower part of the horizontal plexus. An interesting feature shown herein is that cross-sectional views nicely reveal features as a function of depth (Fig. 4). In addition, layer-specific MIPs revealed structural patterns of the skin at different layers under the skin at depths beyond 1 mm. The illumination herein was at 532 nm. Illumination in the visible maximizes label-free imaging of the skin but limits the penetration depth achieved due to the strong light attenuation in tissues. Further work will consist of characterizing the performance of this approach in the near infrared, to achieve deeper penetration. Future steps consist of integrating the system shown in Fig. 3 into a portable format for use in clinics. For this purpose, a redesign is required to enable handheld operation, which is not possible now due to the large size of the motorized stages.

We would like to acknowledge financial support from an ERC Advanced Investigation Award as well as EU FP7 FAMOS and EU Marie Curie IEF fellowships.

References

1. T. L. Group, *The Society for Investigative Dermatology and The American Academy of Dermatology Association* (2005).
2. M. Rajadhyaksha, S. Gonzalez, J. M. Zavislan, R. R. Anderson, and R. H. Webb, J. Invest. Dermatol. **113**, 293 (1999).
3. M. Balu, A. Mazhar, C. K. Hayakawa, R. Mittal, T. B. Krasieva, K. Konig, V. Venugopalan, and B. J. Tromberg, Biophys. J. **104**, 258 (2013).
4. K. Konig, J. Biophotonics **1**, 13 (2008).
5. C. Blatter, J. Weingast, A. Alex, B. Grajciar, W. Wieser, W. Drexler, R. Huber, and R. A. Leitgeb, Biomed. Opt. Express **3**, 2636 (2012).
6. G. Krahn, P. Gottlober, C. Sander, and R. U. Peter, Pigment Cell Res. **11**, 151 (1998).
7. L. C. Junqueira, *Springer-Lehrbuch* (Springer, 2004).
8. V. Ntziachristos, Nat. Methods **7**, 603 (2010).
9. E. Z. Zhang, J. G. Laufer, R. B. Pedley, and P. C. Beard, Phys. Med. Biol. **54**, 1035 (2009).
10. H. F. Zhang, K. Maslov, G. Stoica, and L. V. Wang, Nat. Biotechnol. **24**, 848 (2006).
11. L. Vionnet, J. Gateau, M. Schwarz, A. Buehler, V. Ermolayev, and V. Ntziachristos, IEEE Trans. Med. Imaging **33**, 535 (2014).

12. J. Laufer, P. Johnson, E. Zhang, B. Treeby, B. Cox, B. Pedley, and P. Beard, J. Biomed. Opt. **17**, 056016 (2012).
13. I. M. Braverman and A. Yen, J. Invest. Dermatol. **68**, 53 (1977).
14. E. Zhang, J. Laufer, and P. Beard, Appl. Opt. **47**, 561 (2008).
15. K. Maslov, G. Stoica, and L. V. Wang, Opt. Lett. **30**, 625 (2005).
16. J. Aguirre, A. Giannoula, T. Minagawa, L. Funk, P. Turon, and T. Durduran, Biomed. Opt. Express **4**, 2813 (2013).
17. I. M. Braverman, Microcirculation **4**, 329 (1997).
18. S. Nouveau-Richard, M. Monot, P. Bastien, and O. de Lacharriere, Skin Res. Technol. **10**, 136 (2004).
19. C. P. Favazza, O. Jassim, L. A. Cornelius, and L. V. Wang, J. Biomed. Opt. **16**, 016015 (2011).
20. E. V. Karabutov, A. A. Savateeva, and A. A. Oraesvky SPIE (1999).
21. M. Omar, J. Gateau, and V. Ntziachristos, Opt. Lett. **38**, 2472 (2013).
22. M. Omar, D. Soliman, A. Gateau, and V. Ntziachristos, Opt. Lett. **39**, 3911 (2014).
23. J. Gateau, T. Chaigne, O. Katz, S. Gigan, and E. Bossy, Opt. Lett. **38**, 5188 (2013).
24. G. Liu and Z. Chen, Appl. Opt. **52**, 5473 (2013).

Queries

1. AU: Text unclear here; please clarify.

2. AU: Palm hand correct here?

3. AU: Please provide publisher name for ref. [1].

4. AU: Please provide first page for ref. [20].